The 10th International Conference on Computational Fluid Dynamics (ICCFD10), Barcelona, Spain, July 9-13, 2018

ICCFD10-091

Aerodynamic Design and Optimization of Fan Stage for Boundary Layer Ingestion Propulsion System

Byung Joon Lee* and May-Fun Liou**
Corresponding author: May-Fun.Liou@nasa.gov

NASA Glenn Research Center, USA

Abstract: The present paper addresses the process of preliminary design of low pressure fan and outlet guide vane (OGV) of a boundary layer ingestion propulsion system. The tail-cone thruster systems of NASA's STARC_ABL adopts axi-symmetric BLI type inlet as opposed to other embedded engine systems. Thus, the focus of the present work is placed on maximizing the efficiency of the fan and OGV stages under a significant radial distortion. A parameterization with B-spline function for camber line angles, metal chord, thickness distribution and stacking axis of blades are presented. The flowpath lines are also parameterized by B-spline function and aggregated in the design system of blades. The design optimization with evolutionary algorithm is performed with constraints of fan pressure ratio, OGV exit swirl angle and nozzle exit properties. The inlet conditions for the turbo-machinery CFD domain and the design goal of the fan stage are driven by propulsion airframe integration (PAI) model that uses a 3-D unstructured RANS solver and actuator disk model. The expected power saving of the BLI propulsor is quantified via PAI analysis and the resulting preliminary design of the fan stages is compared with clean inlet flow propulsor.

Keywords: Aerodynamics, Design Optimization, Turbo-electric Fan, Boundary Layer Ingestion, Computational Fluid Dynamics.

1 Introduction

A trend of the next generation aircrafts toward next couple of decades is that the power system is more electric for it benefits of reducing fuel burn, takeoff noise and emission. Hence, more environment-friendly and energy efficient aircrafts of NASA's N+3 generation are planned for entering into service toward the time frame of 2030s and beyond[1]. As part of those efforts, hybrid or fully electric propulsion systems are proposed for NASA's next generation subsonic aircrafts such as STARC_ABL, SUGAR Volt and N3-X. Among those notable concept studies initiated by NASA, STARC_ABL, D8 and N3-X have energy efficiency enhanced by adopting boundary layer ingestion (BLI) propulsion systems. The principal idea of the BLI propulsion is that the propulsor ingests low momentum flow from the wake of the fuselage and generate thrust with less ram drag.

Dr. Meng-Sing Liou had made extensive contributions in expanding the aerodynamic application of the CFD-based design optimization and boundary layer ingestion aircraft design during the last 10 years. His works include Propulsion-Airframe Integration (PAI) design of a low boom supersonic business jet[2], a mitigation of total pressure distortion of boundary layer ingestion inlet[3], thrust maximization of unsteady flapping airfoils[4], and a series of design works of the propulsion-airframe integration for NASA's N3-X aircraft[5-7]. N3-X is proposed to be powered by a turboelectric distributed propulsion (TeDP) system and Liou's last interest was to design a counter rotating fan system as the propulsor for this next generation hybrid wing/body aircraft. Along with the numerous applications, the CFD based aerodynamic design tools developed at NASA Glenn Research Center (GRC) is his great legacy for the next generation aircraft development.

A thorough review of the BLI research in the past has been done in [8] which proposed an approach for building a fully coupled propulsive-aerodynamic models of boundary layer ingestion propulsion systems. Together with [9], they provide system level assessments of the integrated benefit of the BLI propulsion system. The present work aims at developing a preliminary design framework for BLI propulsor by leveraging the existing tools of Propulsion-Airframe Integration (PAI), and turbo-machinery CFD analysis codes. In the development of NASA's STARC-ABL aircraft, its boundary layer ingestion thruster dubbed as tail-cone thruster (TCT), illustrated in Fig. 1, is powered by electric motors and was evaluated at the system level[10], as shown in Fig. 1. The authors and Liou recently proposed a conceptual design of the TCT propulsion system [11] that is based on the system design requirements shown in [10]. Continuing the same effort, the preliminary design and optimization of an axial fan stage of a tail-cone thruster is presented and assessed based on the BLI performance metrics.[12] Hereafter, the essential CFD based aerodynamic tools for the electric and boundary layer ingestion propulsor systems will be introduced in the following sections. Each individual component, including fan, outlet guided van (OGV), and flowpath, of the BLI propulsion system, and its design results in terms of parameterization, and optimization will follow. Finally, assessment of the performance of the fan stage as well as PAI performance will conclude this study.

Figure 1: NASA's Starc-ABL concept aircraft with a hybrid electric propulsion system which includes two turbofan-engines and an aft-mounted BLI propulsor [10].

2 Design of Electric Propulsor under Boundary Layer Ingestion

The previous CFD-based design study using Go-Flow and bodyforce model[13] are shown in Fig. 2. Note that the tail-cone thruster in this study is driven by an electric motor and does not include core engines as shown in Fig. 1. The figure illustrates a PAI analysis comparing the baseline presented in Fig. 2-(a) and with the conceptually designed TCT[11] shown in Fig. 2-(b). Two notable observations can be made from Fig. 2-(a). First, the exhaust cone angle needs to remain benign to prevent jet flow from over-expansion. Second, the low momentum flow at the hub demands a reasonable contraction to accommodate low diffusion factor via acceleration of the flow speed through the fan stage. As a result of making up these two deficiencies, the hub radius at the nozzle got remarkably elevated and needed a stretched exhaust nozzle cone as seen in Fig. 2-(b). In addition, the diffusion of low momentum boundary layer flow throughout the tail-cone reduced the needs for the inlet significantly. Moreover, these features of the conceptual design indicate the need for a strongly coupled design system within propulsion airframe integration. Thus, we have developed a multi-fidelity design frame work aiming at a synthetic design and optimization system including the turbo-machinery modules [11]. The flowchart describing all the modules in the framework is displayed in Table 1. CFD tools used are comprised of two turbo-machinery codes (a quasi-2D through flow and a 3-D single blade as well as multi-stage RANS), and two RANS flow solvers equipped with either actuator disk or bodyforce model. The present task is a continuation of the development of the multi-fidelity design framework described in [11], moving from the conceptual design of an axial fan stages of a TCT type propulsion system into preliminary design. CFD tools exploited in the present study are SWIFT V4.0[12,13] and FUN3D[14]. The SWIFT code is a 3-D RANS turbomachinery analysis code, multiblock, periodic condition for blade to

blade, and utilizing mixing plane between the blade rows and AUSM+[15] was implemented by Liou for the flux function. The flow solver, FUN3D which is a suite of codes for the flow analysis, design and optimization is employed for PAI analysis and design.[9] It uses mixed-element unstructured grids in a various formats, including hexa multi-block and overset grid systems. Its one-equation Spalart-Allmaras turbulence model was chosen for its performance in dealing with external flow. FUN3D has multiple options in different fidelity of model to simulate rotating blade system[14] and mainly used in the present study to simulate the clean inlet flow, i.e., non-BLI propulsion system.

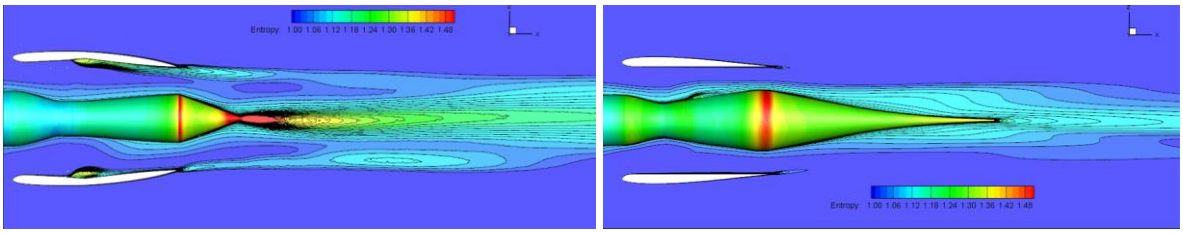

(a) (b)

Figure 2: (a) Baseline Propulsor (FPR=1.25, P=3405HP, MFR=132kg/sec, T=9.67kN), (b) new propulsor design (FPR=1.21, P=3452 HP, MFR=168.7kg/sec, T=11.29kN)

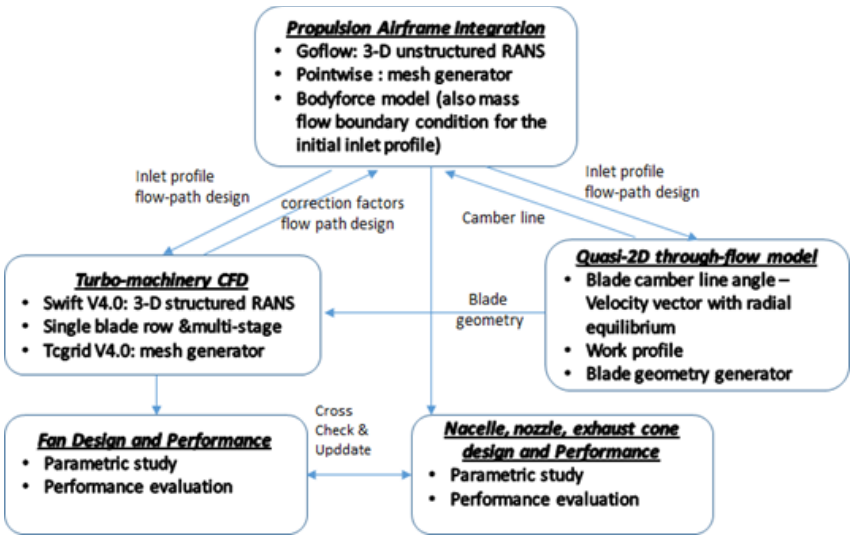

Table 1. Flow chart of the multi-fidelity propulsor conceptual design framework.

Figure 3 shows an example of CFD analyses of the conceptual TCT with bodyforce model and an area equivalent clean flow engine which has the same fan face area and downstream flowpath geometry including the nozzle and exhaust cone. As observed in the comparison of the total pressure contours in Figs.3, the clean flow engine ingests high momentum flow into the inlet and adds work on the downstream flow uniformly. On the other hand, the BLI engine ingests low momentum inlet flow from the wake of the airframe with pressure distortion. Thus, the downstream jet shows lower momentum than that of clean flow engines for the same fan pressure ratio. In addition, the mass flow rate through the propulsor is lower than the clean flow engines. As a result, for the same thrust engines, the BLI engines will need less power as the shaft power is proportional to the product of the ingested mass flow rate and the square of jet velocity. Figure 4 shows the power saving from the CFD analyses. The propulsion system for the clean inlet flow engine is modeled by actuator disk model which does not consider the efficiency penalty from the fan-stages. Thus, the black-dashed curve depicts the minimum shaft power per thrust from the area equivalent clean flow engine. The BLI engines are modeled by turbo-machinery CFD (blue dot) and PAI model using bodyforce (red dot) of the conceptual propulsor design which includes the efficiency penalty from fan/OGV operation.[11] For instance, at a thrust of T_0=

13(kN), the current conceptual design indicated by the red solid line estimates the shaft power requirements, 4,000 (hp). On the other hand, the clean flow engine is estimated to require about 5,000 (hp). Thus, we could expect the SFC saving by 20% (only for 1 engine) via adopting BLI concept with respect to the conventional clean flow engine. However, the efficiency penalty of the fan-stage from the radial distortion degrades the benefit. For the design fan pressure ratio, FPR=1.3, the adiabatic efficiency of the conventional fan-stage at the design pressure ratio reaches about 93% while the conceptual BLI design shows about 88%, thus, about 5% efficiency penalty is expected. At the preliminary stage, the performance gap between the BLI and ideal conventional fan stages originated from the radial distortion penalty will be mitigated.

A special feature of the preliminary design is the addition of a design optimization module which is carried out in terms of the turbo-machinery perspective to mitigate the aforementioned performance gap. The optimization processes start with geometric parameterization of the propulsor and the flowpath. Details are given in the following sub-sections.

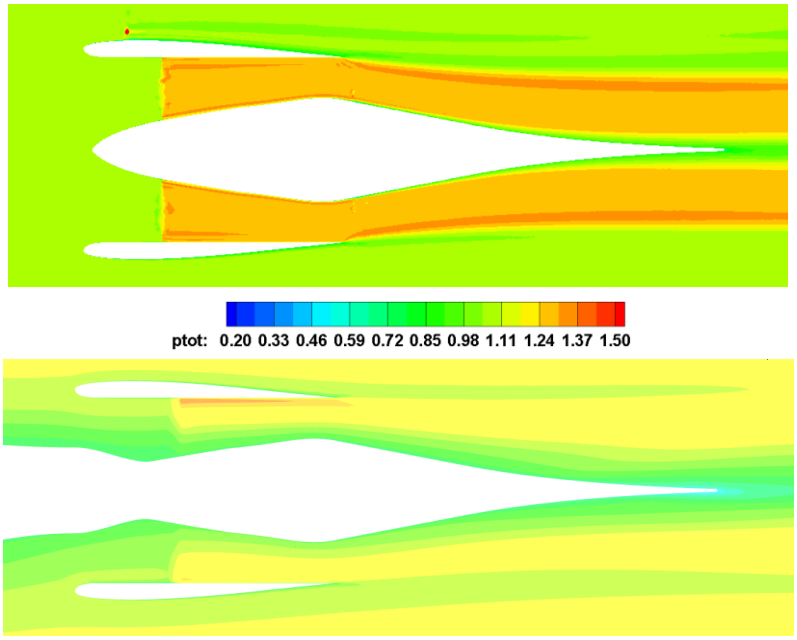

Figure 3: CFD analyses for tail-cone thruster (lower) and clean inlet flow engine (upper) models

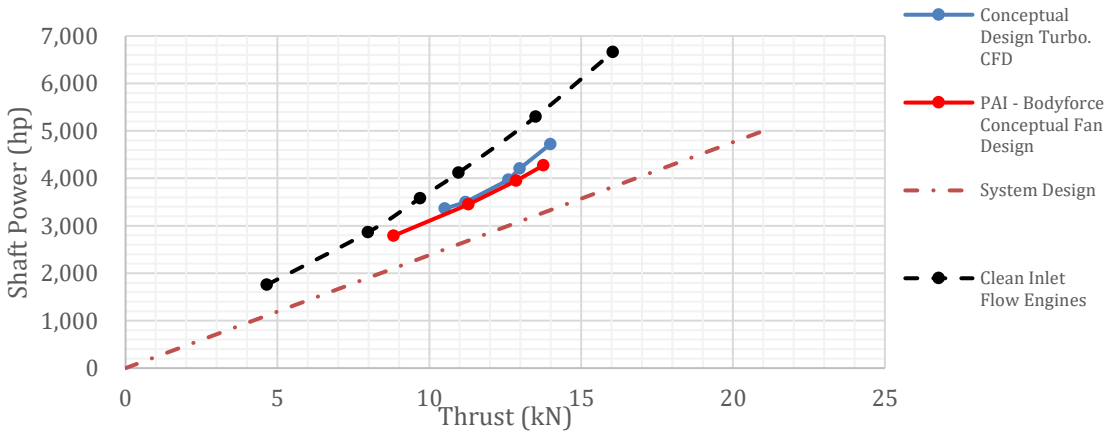

Figure 4: Performance goal and power saving of conceptual design relative to clean inlet flow engine

2-A Parameterization

The baseline metal angles of blades are derived by a quasi-2D through flow model[11]. The distribution of the meanline angles from the conceptual design is parameterized via B-Spline surface

and its %chord versus radius as shown in Figs. 5. Note that %chord is the normalized z-coordinate (axial) in cylindrical coordinate with respect to the metal chord. The grid and black dots depict the distribution of the control points.

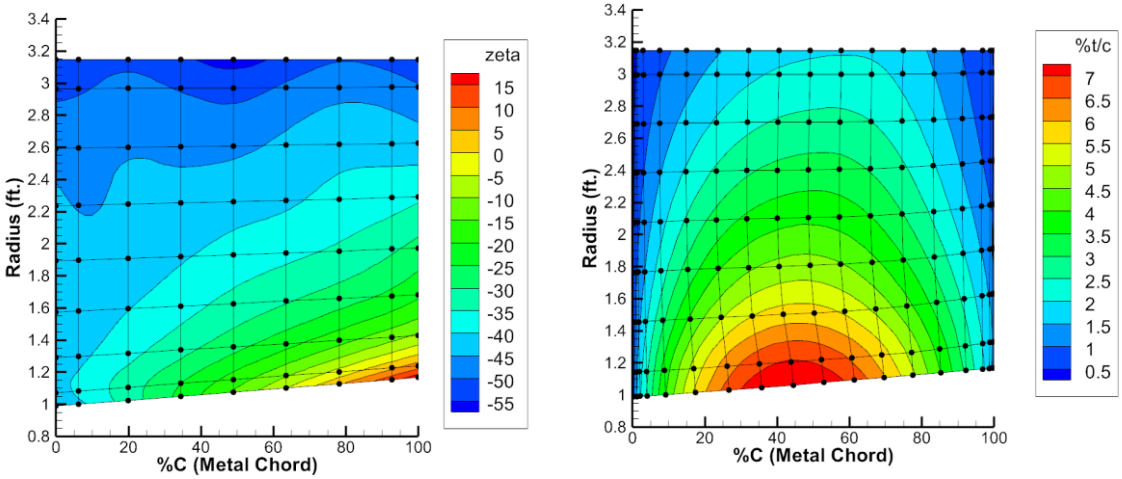

(a) Distribution of camber line angles, ζ [◦]. (b) Distribution of thickness (%t/c).

Figure 5: Parameterization of fan blade

The blade thickness distribution needs to take mechanical design into consideration, thus, the same thickness distribution from the conceptual design is used for the present preliminary design. However, the thickness distribution is parameterized in the code for the optimizations in the detail design. No less than 1 control point within 3% chord distance from the leading and trailing edges per each design section are mandated to control the edge thicknesses as shown in Fig. 5-(b). The blade parameterization code also controls the metal chord length per radial location of each design section. Nose droop is enabled via asymmetric thickness distribution relative to the camber line. The stacking axis is located at the center of gravity of each section for the blades and trailing edge for the vanes respectively. Figures 6 show the geometric outputs from the parameterization of the fan blade and OGV obtained from the conceptual design.

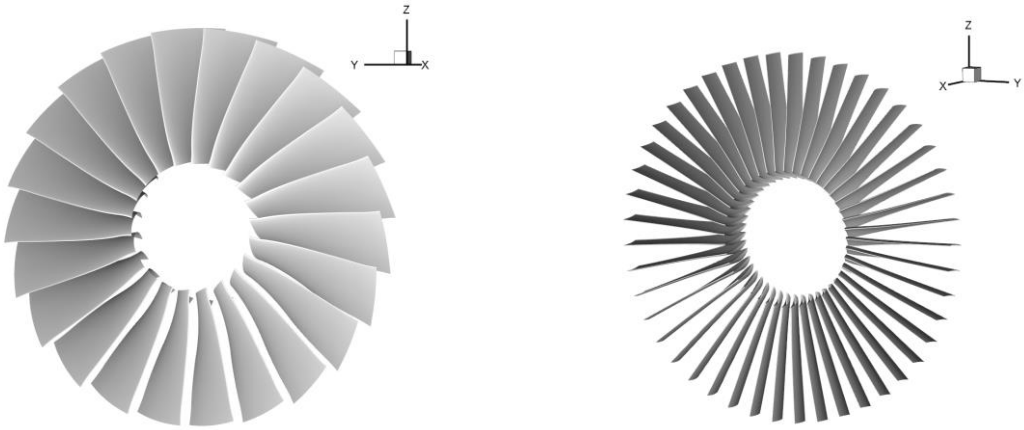

(a) Fan blade (22 counts.) (b) OGVs (45 counts.)

Figure 6: Blade geometries generated by parameterization

As for the internal flow paths including hub and shroud lines are extended upstream to the fuselage lines and downstream to the exhaust cone as shown in Fig. 7. The external line of the nacelle is also parameterized in the same manner but not considered as design parameters in the present design. The number of the control parameters in both blade and flow-path parameterization can be determined per user input. The outputs of the blade and flow-path parameters are automatically translated into the inputs for the mesh generator, TCgrid V4.0, so the process of generating the turbo-machinery meshes is fully automated. Because of the computationally high efficiency of each module in the framework, the whole process from the velocity vector study in quasi-2-D model to the mesh generation shown in the Table

1, takes only about 10 seconds in a conventional work-station environment.

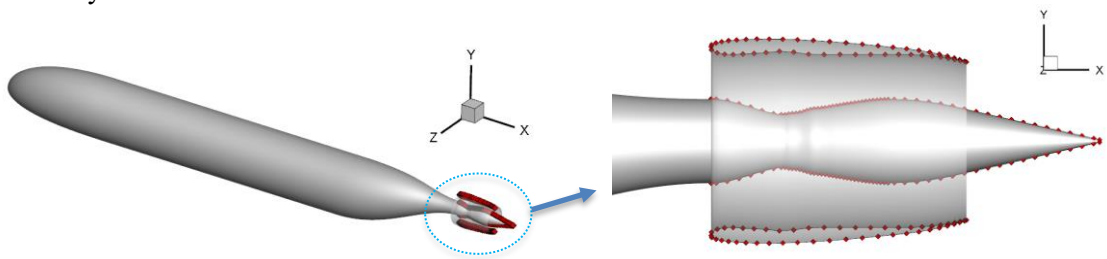

Figure 7: Parameterization of nacelle of the tail-cone thruster, red dots indicating control points.

2-B Numerical Methods

As mentioned above, the CFD analysis for the turbo-machinery module is performed via SWIFT V4.0, a 3-D structured RANS solver with various 0-equation to 2-equation turbulence models. The code takes advantage of openMP for parallel computing, and thus is efficient for distributed direct design analyses when coupled with an evolutionary algorithm. The design is performed using single blade row models for the rotor and stator respectively and the final performance is evaluated through the multi-stage CFD with mixing plane. Figure 8 shows a meridional and blade to blade views of the computational mesh for a multi-stage model. The average Y+ on the blade surface is maintained below 5. The tip clearance is ignored for both conceptual and preliminary designs but its effect is checked in the multi-stage model by comparing the fan exit profiles and speed-line analysis with the no-tip clearance cases.

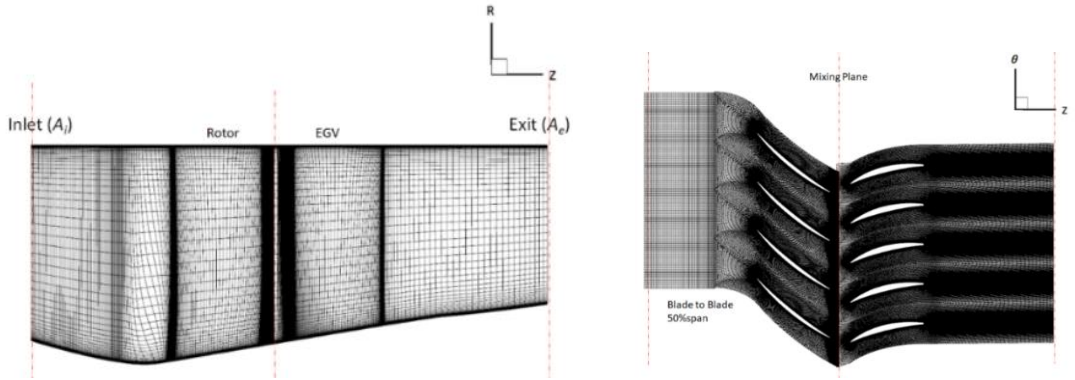

(a) meridional View (b) blade to blade view

Figure 8: The mesh generation from TCGRID V4.0 for SWIFT CFD analysis. On the right, blade to blade view mesh is scaled by 3 along the circumferential direction.

The inlet boundary condition (radial profiles) from PAI CFD model is forwarded to both the quasi-2D and Turbo-machinery CFD modules. As indicated in the Table 1, the PAI analysis is performed by the Go-flow code which is a 3-D unstructured RANS solver and employs bodyforce model to represent the turbo-machinery component in the propulsor, see [7,11] for details. The applied optimizer is NSGA-II[16] which employs a multi-objective genetic algorithm. Inputs required for NSGA-II are population size, generations, number and bounds of design variables, and probabilities of mutation and crossover. Design variables are geometric parameters of blades, flow-path. The design variables are normalized by upper and lower physical limits, thus, bounded between -1 and 1 during the optimization. The objective function of each component is defined and each corresponding optimization result is assessed in the next section.

3 Design and Optimization of Fan Stage

3-A Fan Design

The geometry from inlet to the Aerodynamic Interface Plane (AIP) at z=35m is frozen and is kept as same as the conceptual one [11] because the current study only focuses on the preliminary design of the blades as well as the flow-path. The number of design parameters for the rotor blade is 20 which

consists of 15 mean-line angles (i.e. 3 sections defined at 40%, 75%, 100%span and 5 per each section) and metal chord lengths for 5 design sections which are radially evenly distributed from hub to tip. The stacking axis is automatically updated as the blade shape changes. The objective of the rotor design is to maximize the adiabatic efficiency η_{ad}. The function and its constraints on fan pressure ratio and mass flow rate are described in Eqs. (1)~(3)

$$\text{Maximize:} \quad \eta_{ad} \tag{1}$$

$$\text{Subject to:} \quad (\dot{m_c} - \dot{m_{c,0}})/\dot{m_{c,0}} \leq 0.01 \tag{2}$$

$$(pr - pr_0)/pr_0 \leq 0.005 \tag{3}$$

The design fan pressure ratio is 1.31 and kept within 0.5% band during the optimization. The mass flow rate is 157.87kg/sec and constrained within 1% of variation. The blade count is 22. The tip speed of the fan blade is 1173ft/sec. Figure 9 shows the history of the rotor design with NSGA-II. The efficiency gain through the optimization process is about 3% and the adiabatic efficiency reaches 90%. The static pressure contours of the optimized (on the right) and baseline (on the left) designs in Figs. 10 reveal its corresponding geometry respectively. The baseline geometry is the conceptual one and has the taper ratio of 0.7 determined by CFD parametric study. The strength of the passage shocks at the tip for both pressure and suction sides are fundamentally reduced in the optimized design. The pitch line (at 50%span, the scale %span is the non-dimensional r-coordinate in meridional plane) chord gets longer to improve the pumping of low momentum flow with higher solidity. Leading edge at the tip is forward swept to push the flow to the tip. The blade to blade total pressure contours for selected spanwise locations are shown in Figs. 11. On the right, the trailing edge separation at the 60%span is attached to the blade surface, thus the wake loss is reduced. The change in near tip (95%span) is more remarkable. It is observed in Fig. 11-(b) that the leading edge shock of the optimized design gets more oblique and contained into the passage and the strength of the passage shock gets much weaker than that of the baseline rotor.

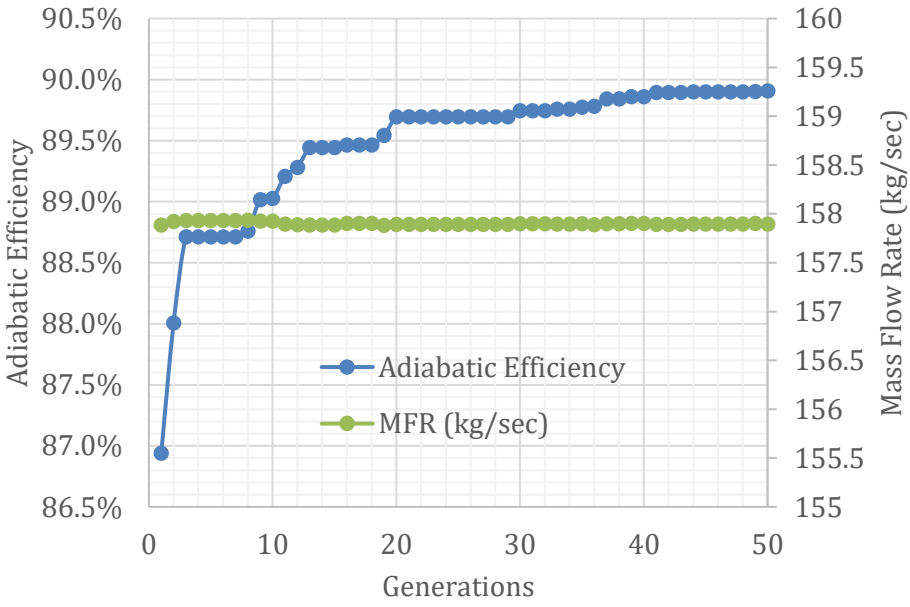

Figure. 9: Design history of fan blade

Figure 12 shows the comparison of the radial efficiency profiles between the baseline and optimized. The biggest efficiency gain is obtained from the 90%span to the tip region due to the mitigation of the shock. In addition, other significant improvement could be observed at 60~70%span as well as at the below 20%span hub region. The change in the radial chord distribution in optimized blade design causes adequate solidity distribution so that the trailing edge separation can be minimized.

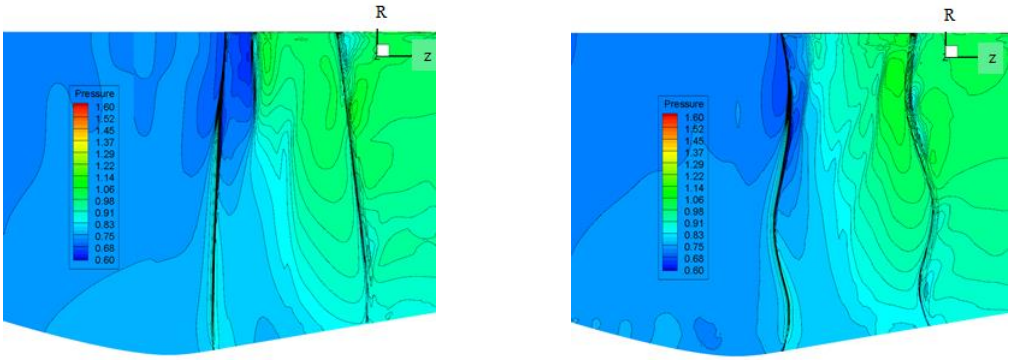

(a) Pressure side (Left: Conceptual Design, Right: Optimized Design)

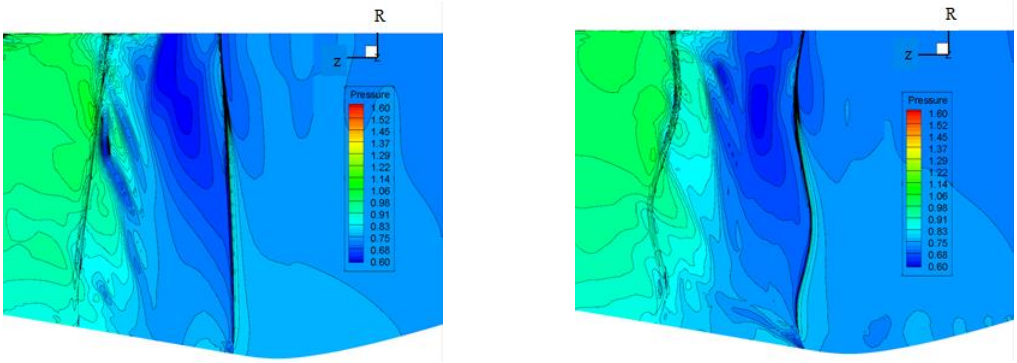

(b) Suction side (Left: Conceptual Design, Right: Optimized Design)

Figure 10. Comparison of static pressure distribution on the blade surface (meridional plane, axial direction: +Z)

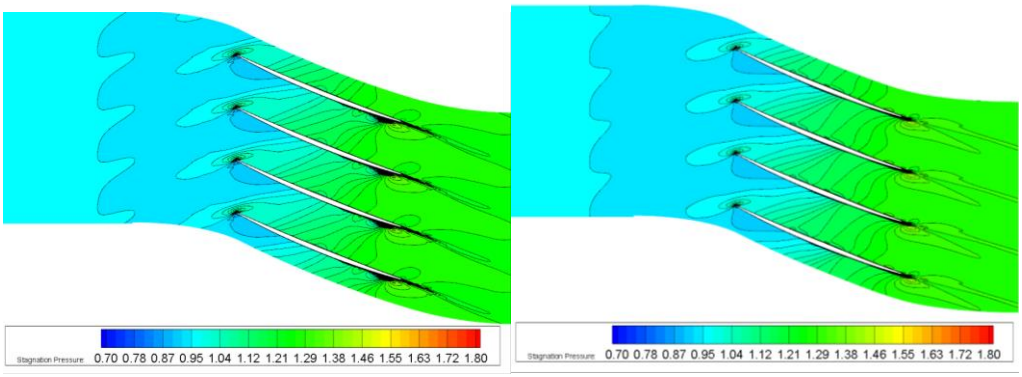

(a) 60%Span (Left: Conceptual Design, Right: Optimized Design)

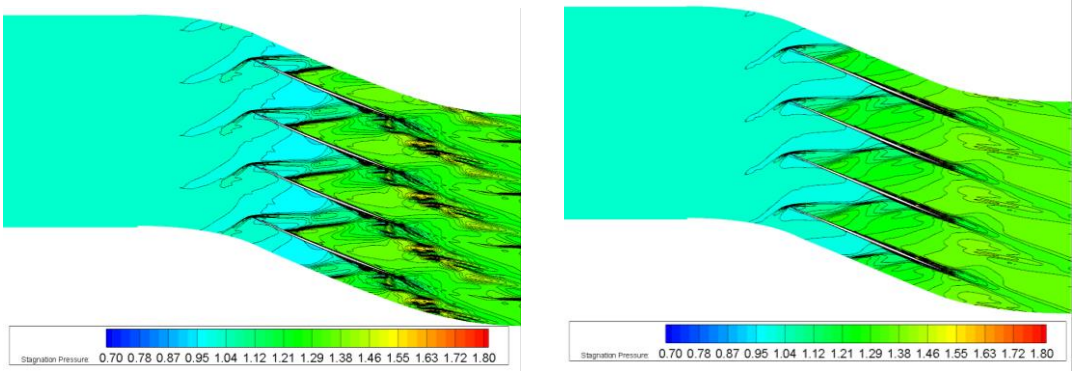

(b) 95%span (Left: Conceptual Design, Right: Optimized Design)

Figure 11. Comparison of blade to blade total pressure contours ($z - \theta$ plane, *θ not scaled*)

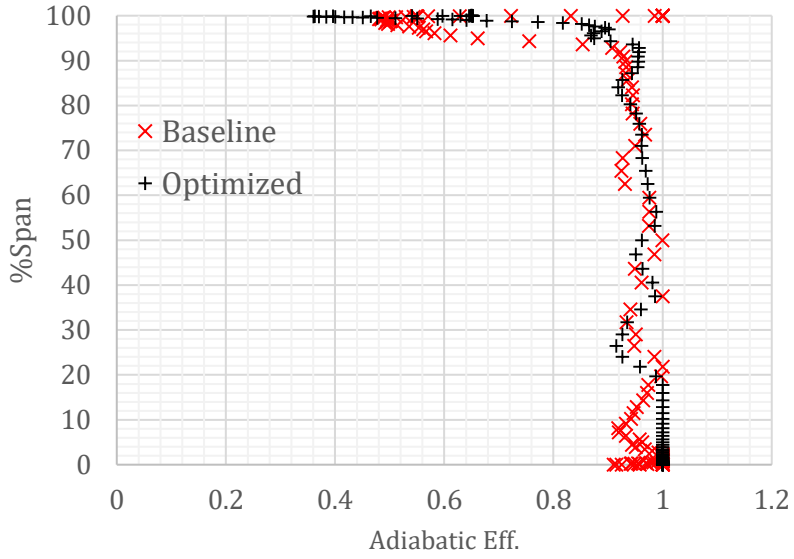

Figure 12: Comparison of radial efficiency profiles

3-B Flowpath Design

Even though the above efficiency profile of the optimized fan indicates the performance improvement for the overall spanwise locations, it is noted that the 20%~50%span region still suffers from the loss caused by trailing edge separation. One way to minimize the hub loss without losing the efficiency gain near tip is to re-design the flowpath. Thus, the hub flowpath parameters are applied to accelerate the low momentum flows moving through fan blades. The tighter flowpath will tend to choke at fan stage earlier than the already optimized fan. So the blade count study is also performed along with the flowpath modification. Figure 13 presents the flowpath change to accommodate the area rule at the fan hub region. The resulting length of nacelle casing is shortened as the nozzle throat location is moved upstream.

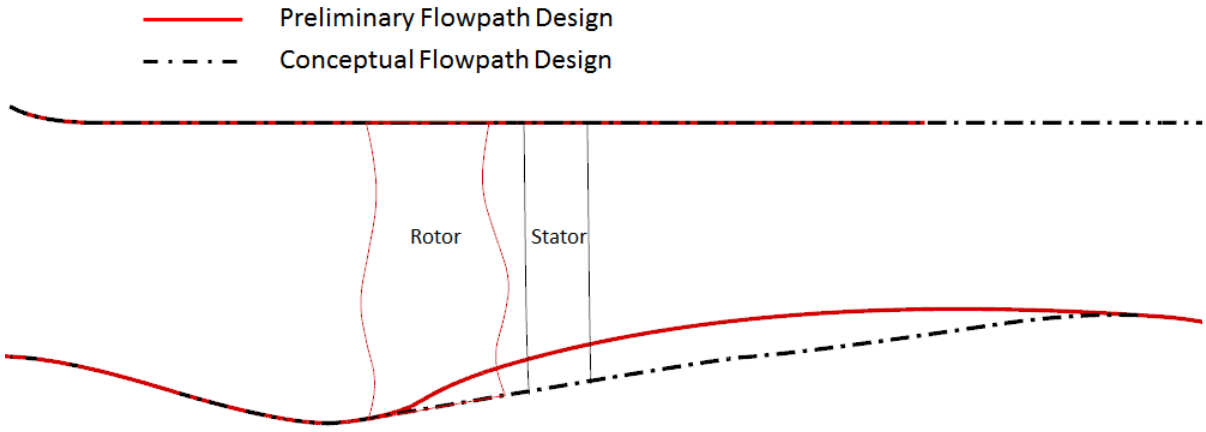

Figure 13. Comparison of flowpath design (in meridional view) between designs

As the flowpath area gets tighter, the blade count is reduced from 22 to 18 to prevent the choking at the fan stage. The fan pressure ratio and mass flow rate are maintained at FPR=1.31, and MFR=158kg/sec respectively. The adiabatic efficiency ramped up to 91.9%. Figure 14 compares the efficiency profiles from the optimized fan blade with and without area rule as well as the conceptual design. The efficiency from the hub up to around 90%span could be improved significantly but gets a penalty near the tip location between 95~97%span relative to the optimized fan.

The total pressure contours in blade-to-blade domain at 30% and 95%spans are compared between optimized fan before and after flowpath change in Fig. 15. The pressure rise with hub contraction is significantly larger than the case before the flowpath change as shown in Fig. 15-(a). On the other hand,

the lower solidity at the tip tends to cause trailing edge separation has raised at the suction side in Figs. 15-(b), thus, the pressure rise is not as good as the optimized fan. However, the difference looks local while the efficiency gain at the hub is remarkable. The tip characteristics of the fan may affect the tip leakage problem, thus, further studies for the tip clearance and solidity will be re-visited in the sections 4 with multi-stage modeling.

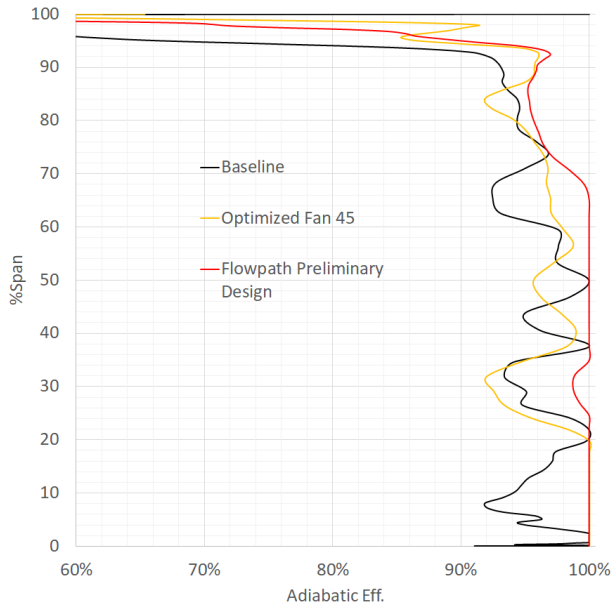

Figure 14. Comparison of efficiency profiles after the flowpath area rule.

3-C OGV Design

The optimized fan stage and the area ruled flowpath have resulted in the need of re-designing the OGV. Based on the incoming flow profile from the optimized fan, OGV performance is assessed and re-designed accordingly. As the fan pressure ratio is low, the critical factor for the OGV loss is the diffusion factor. Thus, the metal chord lengths at nine spanwise locations are employed to optimize the diffusion throughout the OGV stations. In addition, the flowpath is designed to prevent excessive diffusion at the hub region. The velocity vector study from the quasi-2D model has constraints to restricts the OGV trailing edge angle to turn the flow back to the axial direction. Following the empirical blade count relationship for minimum excitation of acoustic waves between rotor and stator[17], 37 vane counts is chosen. The nozzle area is determined via Mach number constraint of $M \leq 0.8$. Figure 16 compares the entropy contours which indicates the source of the pressure loss on the OGV surfaces and in the downstream duct. Fig. 16-(a) shows that the leading edge expansion at suction side of the conceptual design is controlled by the leading edge sweep. The healthier incoming hub flow from the rotor helped to mitigate the loss from the blade as well as the duct significantly. The total pressure loss (%dp/p) from the fan exit to the nozzle through OGVs is reduced from 2.3% to 1.38% through the flowpath design and the optimization of the spanwise chord distribution. The conceptual OGV design is stacked on center of gravity while the preliminary design is stacked at the trailing edge per mechanical consideration. The change of stacking axis contributes the reduction of the wake loss as well.

4 Performance Assessment

The preliminary design of a tail-cone thruster has realized an about 4% increase in the fan blade adiabatic efficiency based on the single blade row CFD. In the present section, the assessments based on multi-stage CFD with mixing plane are conducted to investigate the effect of the tip clearance on the performance of the fan stage, and the performance of the whole thruster system in terms of thrust and shaft power. In addition, the performance maps of the designed fan stage are also presented in the following sub-sections.

4-A Tip Clearance effect and Performance Map

The reduction of fan blade count to prevent early choking resulted in low tip solidity and trailing edge separation locally at 96~100%span region. Furthermore, this count change may increase the detrimental effect of tip clearance leakage. Thus, the tip clearance effect on the preliminary design is investigated during the assessment of the stage performance. The fan diameter is 75.55 inches and the hub to tip radius ratio is 0.32. Figures 17 and 18 compare the rotor and stage performance with different tip clearance level, i.e., ΔS_{tip} = 0.1, 0.2 and 0.3 (inches). The ratios of the tip clearance with respect to the blade height are 0.4%, 0.8% and 1.2% respectively. Figure 17 compares fan pressure ratio per physical mass flow rate (MFR) for rotor and stage. Note that all mass flow rate conditions in the present paper are physical values at the design altitude, not the corrected properties. Figure 18 presents the fan efficiency versus mass flow rate. The peak efficiency is found at MFR=157kg/sec which nears the design condition, and the adiabatic fan efficiency reaches about 92% with tip clearance, ΔS_{tip}<0.2 (in.). Thus, the efficiency penalty from tip clearance is marginal in these studied clearance levels. However, the case of tip clearance ΔS_{tip}=0.3 shows about 1% less efficiency for both rotor and stage. The stage efficiency is about 87%. As the tip clearance increases, the stall incepts earlier than the tighter clearance cases. Figure 19 illustrates the pressure ratio profiles of different tip clearance levels at peak efficiency. Single blade row (SBR) CFD result is included as a reference. The profiles reveal that the SBR CFD predicts pressure ratio higher than the multi-stage (MS) CFD does. This observation is consistent with that the overall fan pressure ratio in the fan map (FPR=1.28) is predicted lower than the fan pressure ratio (FPR=1.31) predicted by SBR CFD. The tip clearance effect is clearly illustrated but the pressure loss from the tip leakage affects higher rotor reaction region (at 90%~95%span) which in return compensates the pressure loss at the very tip. However, the hub pumping (< 10%span) in the no tip clearance case is more favorable than the wide clearance cases, as shown in Fig. 19.

4-B Achievement in Power Saving from Preliminary Propulsor Design

The operating conditions from the fan performance map are presented in the BLI thruster performance map to account for the power saving of the current design relative to the ideal clean inlet flow engine in Fig. 20. The red solid dots indicate the thrust estimation from the present preliminary design of the tail-cone thruster. At the thruster design conditions which are FPR=1.3, and MFR=158kg/sec at 40kft altitude, the BLI engine requires about 3MW (4083HP) to generate 17.8 kN of thrust. For the same thrust generation, the clean flow engine requires over 5MW (6700HP) based on Fig. 4. Thus, the shaft power saving is about 40% (for 1 engine). As the tail-cone thruster is required to provide 33% of the thrust requirement of STARC_ABL, over 13% of fuel burn saving for the aircraft system is expected for the preliminary fan stage design.

5 Conclusion and Future Works

A preliminary design of the BLI propulsor for STARC_ABL aircraft is carried out. The fan stage geometries are parameterized by B-spline for each component of geometry definition, i.e., camber-line, thickness distribution, stacking axis and chord of blades, and flow-path lines, respectively. Based on the conceptual design and multi-fidelity design framework, the baseline geometry is designed to maximize the efficiency with mass flow rate and fan pressure ratio constraints. The performance of the new design is assessed via multi-stage CFD model. The thrust estimation for the design shaft power meets the system design requirements and the performance benefit of the BLI engine relative to the conventional clean inlet flow engine is demonstrated via CFD analyses. However, the present design is assuming axi-symmetric distortion, thus, further efficiency penalty is expected when the vertical stabilizer and wings are installed on the configuration. In addition, the inlet flow profile is not updated according to the change in thruster design, thus, the ram drag update may not be physically correct. Thus, a more rigorous physical modeling such as performance cross-check by high fidelity PAI models is required. The preliminary design of fan stage of an electric BLI propulsor is successfully demonstrated via CFD modeling. High fidelity validation in propulsive performances of the present

design, and detailed design with multi-disciplinary optimization techniques will be carried out for the future works.

Acknowledgement

In memory of the late Dr. Meng-Sing Liou, the authors sincerely appreciate our mentor and like to honor his passion and dedication to the development of the next generation subsonic aircraft with boundary layer ingestion propulsion. We also appreciate financial support of NASA's AATT project and Mr. William Haller, the technical lead of the SA&I subproject. Special thanks to UPAI sub-project team members, Dr. Mark Celestina (propulsion technical lead) for the discussion of the direction of propulsor design, Dr. Christopher Hughes (sub-project manager) for the project support.

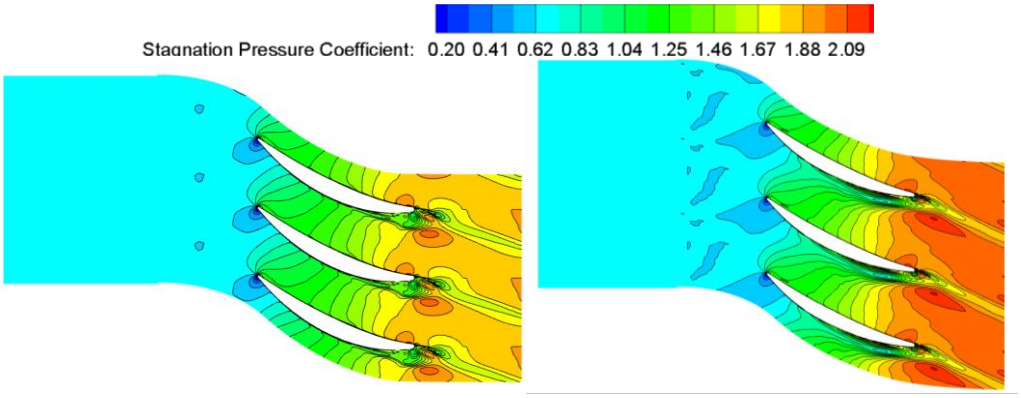

(a) 30%span (Left: without and Right: with flowpath area rule)

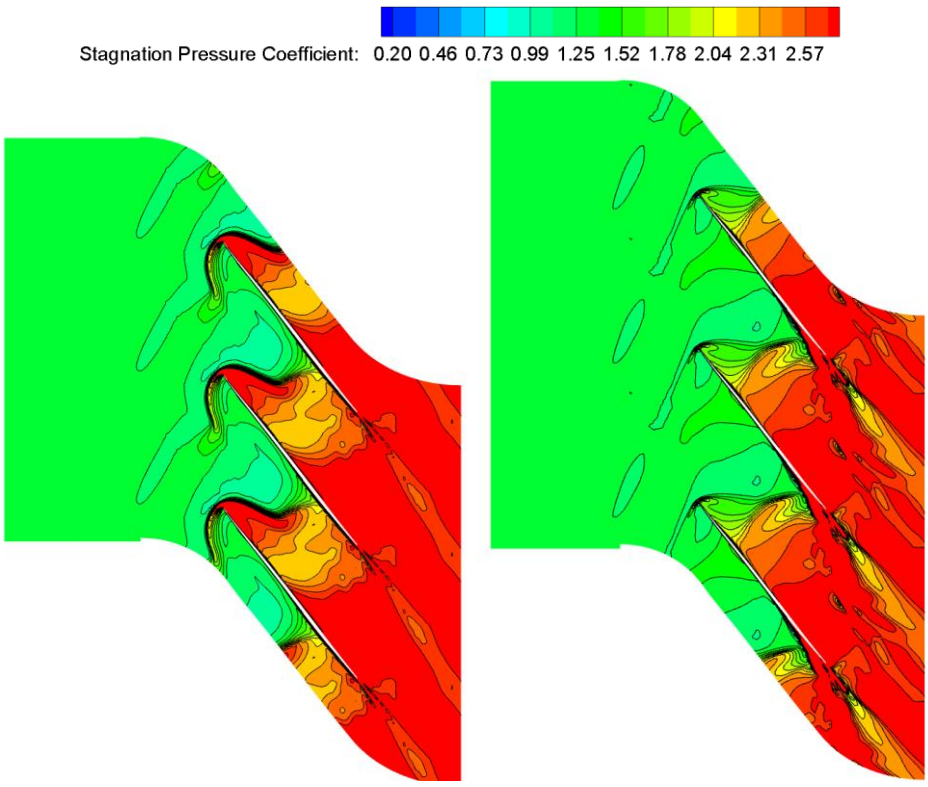

(b) 97.5%span (Left: without and Right: with flowpath area rule)

Figure 15. Comparison of total pressure contours at select %span locations. ($z - \theta$ plane, *θ is scaled for corresponding radius of each section.*)

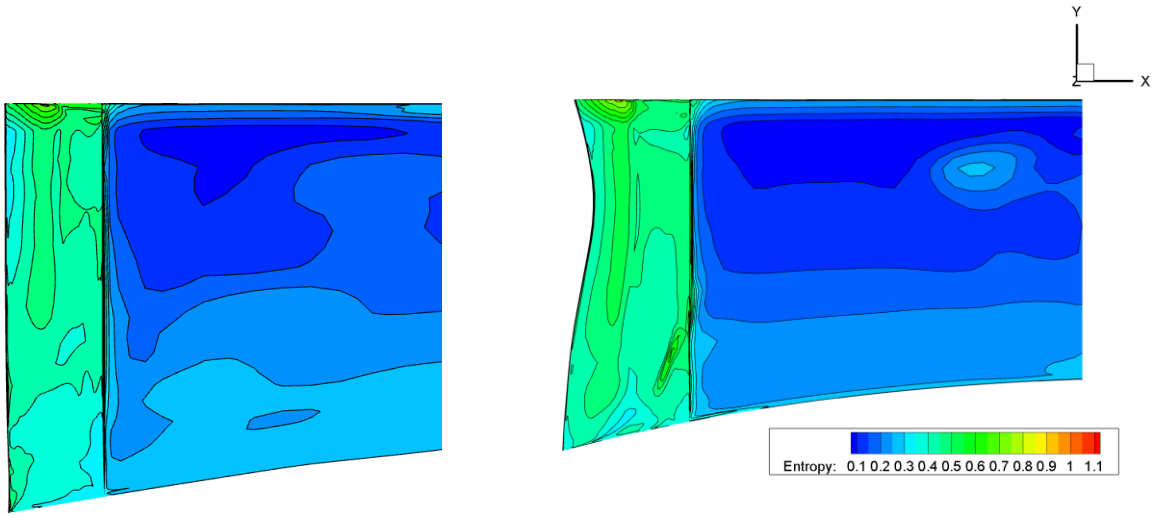

(a) Suction Side (Left: Conceptual Design, Right: Preliminary Design)

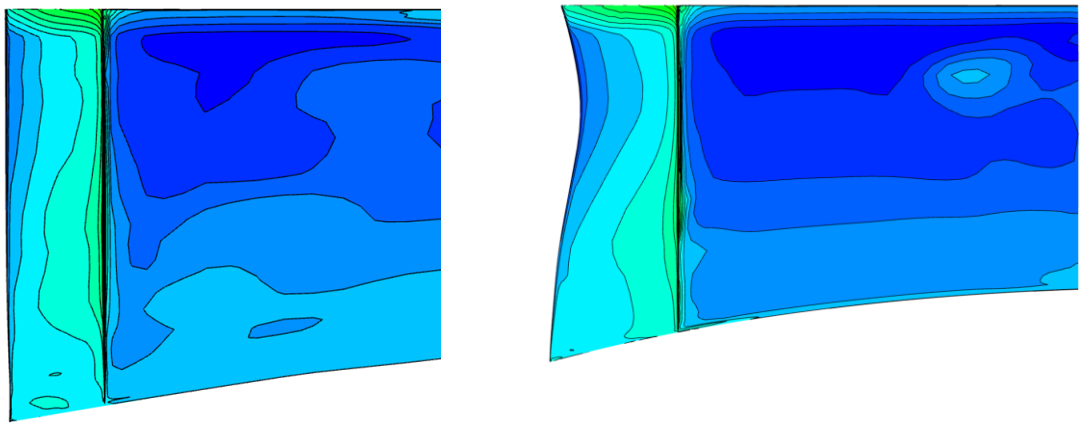

(b) Pressure Side (Left: Conceptual Design, Right: Preliminary Design)

Figure 16. Comparison of entropy contours through the OGV stations

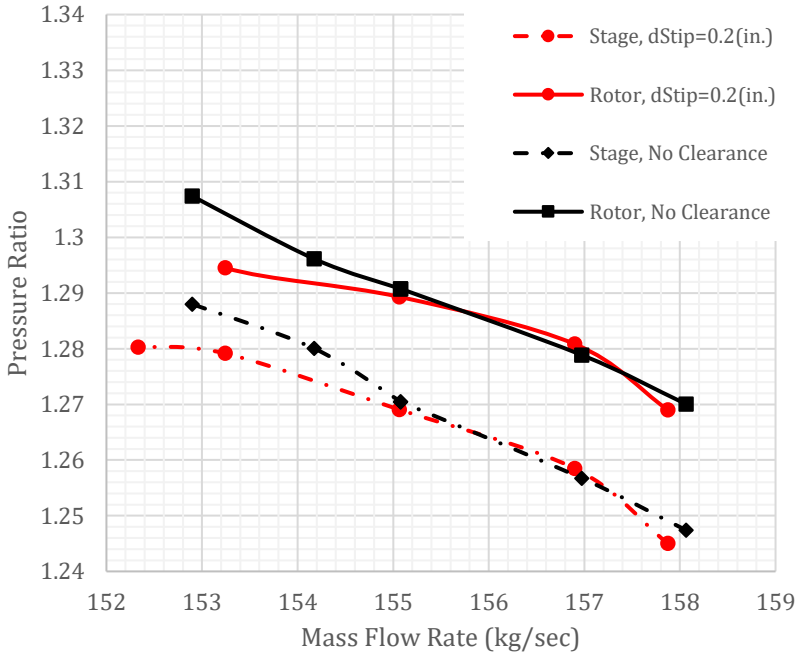

Figure 17. Fan and Stage Performance Map (Pressure ratio vs Mass Flow Rate)

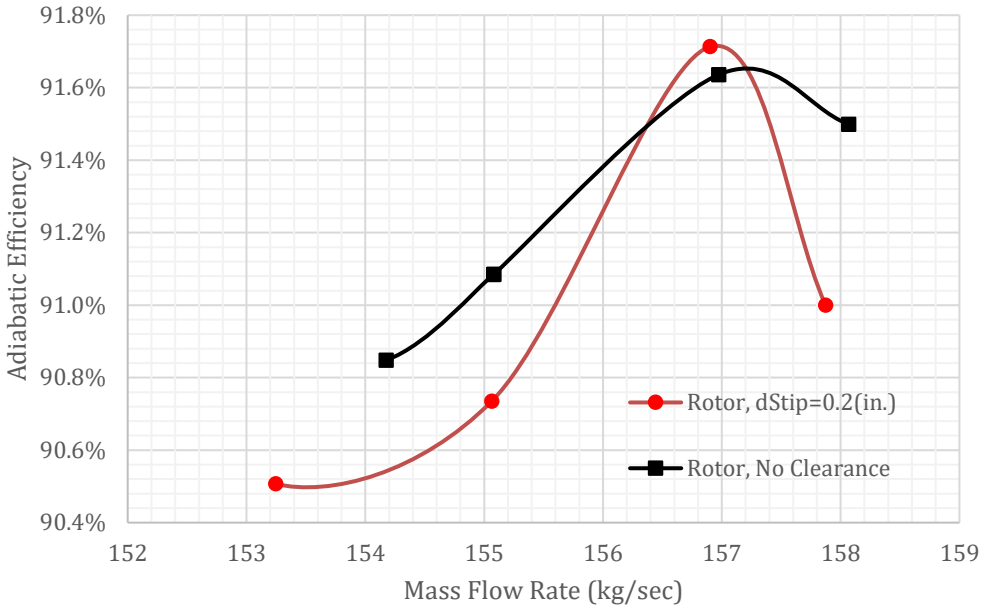

Figure 18. Fan Efficiency Map

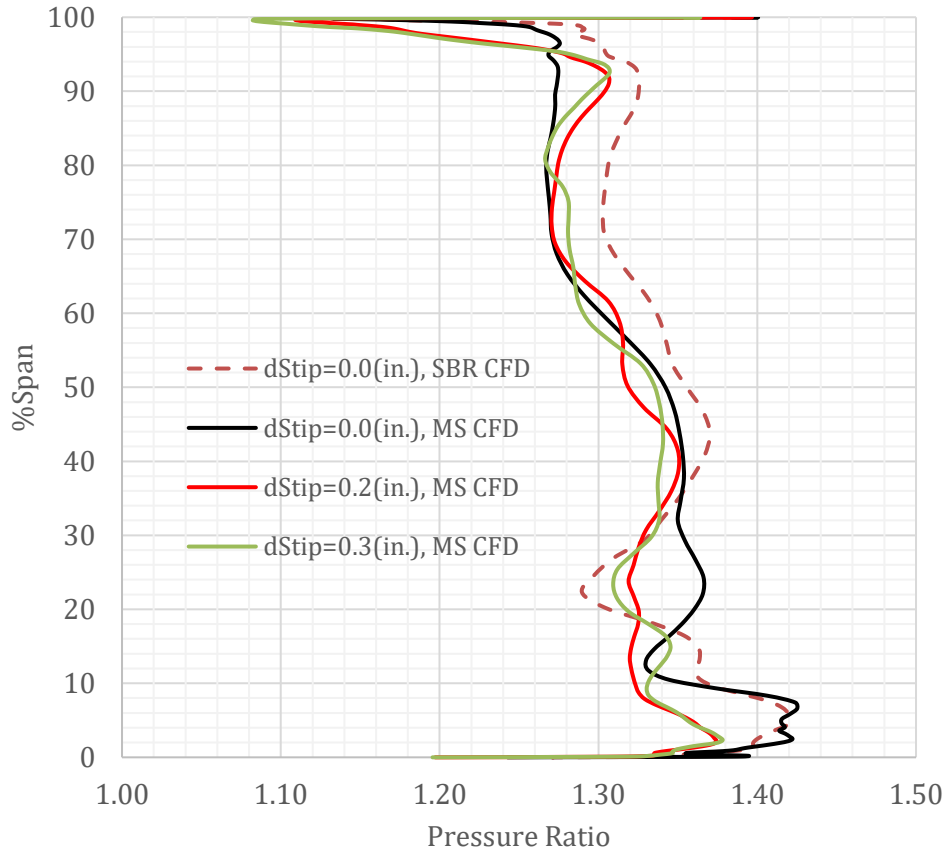

Figure 19. Comparison of Pressure Ratio Profiles for different clearance level at Design Condition (MFR=157kg/sec), where dStip represents ΔS_{tip}.

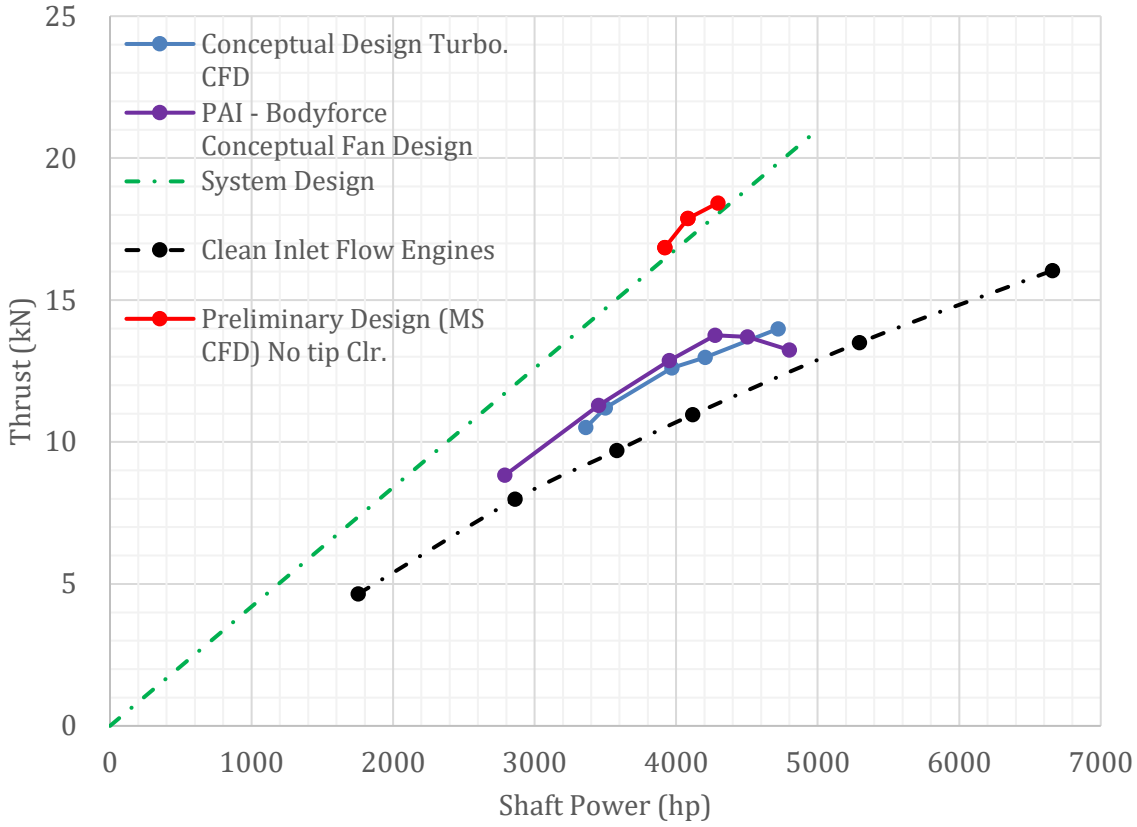

Figure 20. Thrust generation vs shaft power for the tail-cone thruster

References

[1] *Commercial aircraft propulsion and energy systems research: reducing global carbon emissions*, National Academies Press, 2015.

[2] Kim, Hyoung Jin, T. Kumano, Liou, Meng-Sing, and Povinelli, L., "Optimal Bypass Shape Design of Low Boom Supersonic Inlet," The 29th AIAA Applied Aerodynamics Conference, Honollulu, Hawaii, 27-30 Jun, 2011. DOI:10.2514/6.2011-3191

[3] Liou, Meng-Sing, and Lee, B., "Minimizing Inlet Distortion for Hybrid Wing Body Aircraft," *Journal of Turbo-machinery*, Vol. 134, Issue 03, May 2012.

[4] Lee, B. and Liou, Meng-Sing, "Unsteady Adjoint Approach for Design Optimization of Flapping Airfoils," *AIAA Journal*, Vol. 50: 2460-2475, 2012, DOI: 10.2514/1.J051663

[5] Kim, H., Liou, M.-F. and Liou, Meng-Sing, "Mail-Slot Nacelle Shape Design for N3-X Hybrid Wing Body Configuration," AIAA 2015-3805, AIAA Propulsion & Energy Forum 2015, Orlando, FL, 27-29 July, 2015.

[6] Liou, M-F, Kim, H., Lee, B. and Liou, M-S "Aerodynamic Design of Integrated Propulsion-Airframe Configuration of the Hybrid Wingbody Aircraft," AIAA 2017-3411, Aviation Forum, 5-9, June, 2017.

[7] Kim, H.J., and Liou, M.-S. "Flow simulation and optimal shape design of N3-X hybrid wing body configuration using a body force method," Aerospace Science and Technology, Oct, 2017.

[8] Gray, J. S., Mader, C. A., Kenway, G. K.W., Martins, Joaquim R. R. A. "Approach to Modeling Boundary Layer Ingestion using a Fully Coupled Propulsion-RANS Model," AIAA-2017-1753, 58th AIAA/ASCE/AHS/ASC Structures, Structural Dynamics, and Materials Conference, AIAA SciTech Forum.

[9] Lee, B., Liou, M-F, and Kim, H. , "Design of Distributed Mail-slot Propulsion System on a Hybrid Wingbody Aircraft," AIAA 2018-3954, Aviation Forum, 25-29, June, 2018.

[10] Welstead, J. R. and Felder, J. L., "Conceptual Design of a Single-Aisle Turboelectric Commercial

Transport with Fuselage Boundary Layer Ingestion," 54th AIAA Aerospace Sciences Meeting, AIAA 2016-1027, 2016. doi:10.2514/6.2016-1027
[11] Lee, B., Liou, M-F and Liou, M-S, "Multi-Fidelity Aerodynamic Conceptual Design Framework for a Tail-Cone Thruster," GT2018-75861, ASME Turbo Expo, 11-15, June, 2018.
[12] R.V. Chima, "A Three-Dimensional Unsteady CFD Model of Compressor Stability," GT2006-90040, ASME Turbo Expo 2006, Power for Land, Sea, and Air, 8-11, May, 2006.
[13] R.V. Chima, "SWIFT Code Assessment for Two Similar Transonic Compressors," AIAA 2009-1058.
[14] FUN3D Manual V12.7, NASA TM-2015-218761, May 2017.
[15] Liou, M.-S., and Steffen Jr. C. J., "A New Flux Splitting Scheme," J. Computational Physics, Vol. 107, No. 1, July 1993, pp 23-29.
[16] Deb, K. Agrawal, S., Pratap, A., Meyarivan, T., "A Fast and Elitist multi-objective Genetic Algorithm: NSGA-II," IEEE Transactions on Evolutionary Computation (IEEE-TEC), Vol.6, No.2, pp.182-197, 2002.
[17] Hughes, C.E., "Aerodynamic Performance of Scale-Model Turbofan Outlet Guide Vanes Designed for Low Noise," AIAA-2002-0374, Also NASA/TM-2001-211352, 2011.